Ocean Engineering 95 (2015) 183–194

Contents lists available at ScienceDirect

Ocean Engineering

journal homepage: www.elsevier.com/locate/oceaneng

Power-saving device for air bubble generation using a hydrofoil to reduce ship drag: Theory, experiments, and application to ships

Ichiro Kumagai [a,*], Yoshiaki Takahashi [b], Yuichi Murai [c]

[a] School of Science and Engineering, Meisei University, Hino, Tokyo 191-8506, Japan
[b] R&D Engineering Inc., Setagaya-ku, Tokyo 154-0015, Japan
[c] Laboratory for Flow Control, Faculty of Engineering, Hokkaido University, Sapporo, Hokkaido 060-8628, Japan

ARTICLE INFO

Article history:
Received 30 March 2013
Accepted 30 November 2014
Available online 7 January 2015

Keywords:
Ship
Drag reduction
Hydrofoil
Multiphase flow
Bubble

ABSTRACT

We have developed a new power-saving device to reduce the drag of a ship's hull using small bubbles. The device reduces the energy required for bubble generation. The device, which consists of angled hydrofoils with air introducers, uses the low-pressure region produced above the hydrofoil as the ship moves forward to drive atmospheric air into the water. We describe the device principles obtained from simple fluid dynamic theory, and, through experiments performed in a small towing tank, show the fundamental air entrainment and bubble generation processes for the flow behavior around a hydrofoil beneath a free surface. We also present a semi-empirical scaling process for practical application to full-size ships to estimate the net drag reduction achieved by this device. Finally, the results of a series of full-scale tests are reported and show that, with correct operation, our device can produce a net power saving of 5–15% for ships.

1. Introduction

Over the past few decades, the mechanism of air lubrication has been investigated for reduction of the friction drag on a ship's surface and to reduce CO_2 emissions. Three physically different air lubrication techniques have been identified: air cavity, air film, and small bubble methods. The classification of the working principle in these different drag reductions was explained by Ceccio (2010). The small bubble method, which utilizes functions of micro- to sub-millimeter bubbles, has an advantage over the air cavity and air film-based methods in that it reduces friction without requiring any change in the form of the ship's hull. Another advantage is its large impact to the drag reduction ratio per void fraction supplied into the boundary layer. The impact is ordinarily larger than unity, and reaches 100 on ideal conditions as reviewed by Murai (2014). Researchers in this field use the term "microbubble drag reduction" as they expect turbulence modification realized by eddy-suppressing small bubbles inside turbulent boundary layer. Practical application of microbubble method to ship drag reduction has been actively studied in recent years because of the potential energy savings and the environmental benefits in terms of marine pollution. Kodama et al. (2008) reported approximately 10–15% saving of the total energy consumption for an experimental ship. Mizokami et al. (2010) also succeeded in about 10% fuel saving as bubbles were injected below a vessel with wide flat bottom surface. Their ships of air lubrication system are already in commercial uses. For challenging further improvement of drag reduction, Mäkiharju et al. (2012) proposed high-void fraction type of air-layer drag reduction and estimated its usefulness to large tankers. Jang et al. (2014) also reported 5–6% net power-saving estimated for a bulk carrier as they scaled their towing model ship experiments considering the power for bubble injection.

One of concerns toward further improvement of microbubble method is the fact that the energy required to supply air bubbles using conventional bubble generators is quite significant, and it occupies 3–10% of the total energy consumption of a ship dependent on the depth of bubble generation. This explains that the required power for bubble generation in worse operations cancels out the power saved by drag reduction. For example, the theoretical estimate of the energy loss due to the adiabatic compression of air, i.e., the ratio of the internal energy increase ΔU to the work done in the adiabatic compression of air L_{total}, is given by

$$\frac{\Delta U}{L_{total}} = \left(\frac{K-1}{K}\right)\frac{C_V}{R}, \tag{1}$$

where C_v, R, and κ are the heat capacity at constant volume, the gas constant, and the heat capacity ratio, respectively. From Eq. (1), the energy loss due to the adiabatic compression of air is approximately 71% at 20 °C (R=287 J kg^{-1} K^{-1}, C_v=718 J kg^{-1} K^{-1}, and

Abbreviations: WAIP, winged air induction pipe; AIP, air induction pipe

* Corresponding author. Tel.: +81 42 591 9619.
E-mail address: ichiro.kumagai@meisei-u.ac.jp (I. Kumagai).

http://dx.doi.org/10.1016/j.oceaneng.2014.11.019

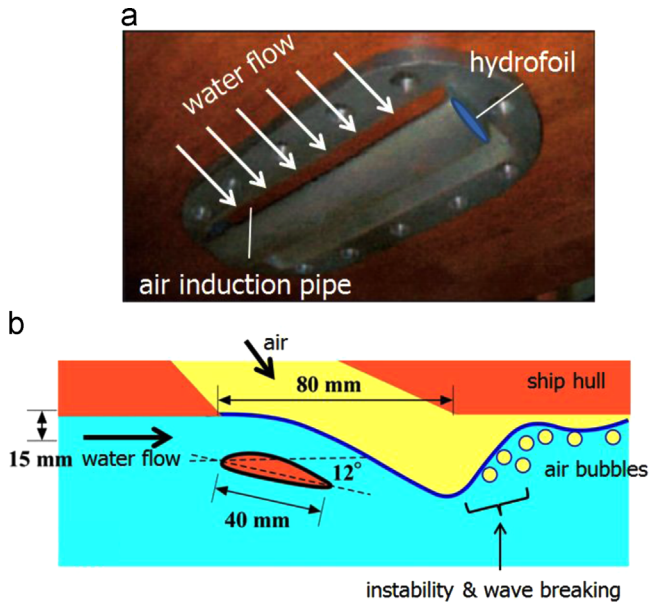

Fig. 1. Winged air induction pipe (WAIP): (a) photograph; (b) schematic drawing of the WAIP cross-section. The hydrofoil is a NACA 65_3-618 (chord length of 40 mm, span-wise length of 240 mm, and angle of attack $\theta=12^\circ$).

$\kappa=1.4$). To supply air bubbles at a specified water depth, the energy required includes the adiabatic compression energy, the energy required for the bubble generation procedure (e.g., the small air bubbles are generated by passing air through either a porous medium or capillary tubes) and the mechanical energy loss in the compressor. As a result, the net power saving declines to as little as 0–5%, which is a serious obstacle to the practical application of microbubbles in the shipbuilding industry (e.g. Kodama et al., 2008).

To overcome this obstacle, we invented a new bubble generation device suitable for its installation to ship (Takahashi and Murai, 2004; Murai and Takahashi 2008). Fig. 1 shows the new device, which is called a winged air induction pipe (WAIP). This device, which has an angled hydrofoil with an air introducer, provides the low-pressure region above the hydrofoil as the ship moves forward. The low pressure drives the atmospheric air to a critical water depth without significant air compression, depending on the flow conditions around the hydrofoil, the hydrofoil's shape, the angle of attack, and other factors. Interaction between the hydrofoil and upper deformable free surface was investigated by Duncan (1983). In our case, the hydrofoil is located at a small distance from the flat wall so that air and water join smoothly to flow out downstream. This device also generates small bubbles without the use of bubble fragmentation devices such as porous plates. We confirmed that the small bubbles are generated by the instability of the air–water interface, which is subject to a high shear rate along the surface of the hydrofoil. The number density of bubbles increases with the subsequent wave-breaking phenomenon which occurs just behind the hydrofoil (Kumagai et al., 2010). We installed WAIPs on a coaster and achieved a net power saving of 10–15% as being elaborated in Sections 4.3 and 4.4 in this paper.

Here, we describe the theory of the entrainment of air by a hydrofoil moving beneath an air–water interface and experimentally demonstrate the bubble generation processes in laboratory scales. We also show a semi-empirical scaling process for estimation of the total drag reduction for ships that can be achieved by installing the WAIP device; the scaling is based on experimental results from a circulating water channel. Finally, we report on full-scale sea trials to demonstrate how our device works in practical applications, which will provide information to optimize the device and lead to further improvements.

2. Theory

2.1. Threshold of air entrainment by a hydrofoil beneath a free surface

When the hydrofoil of a WAIP attached to a ship's hull moves at a constant velocity U, water flows over the hydrofoil surface; a low-pressure region is then produced over the upper surface of the hydrofoil (Murai and Takahashi, 2008). The magnitude of the negative pressure ΔP depends on the flow speed, type of hydrofoil, the angle of attack, and also the depth of the hydrofoil from the air–water interface. The atmospheric air is entrained when the magnitude of the negative pressure is higher than the hydrostatic pressure of the water at the depth of the WAIP installation (Murai et al., 2010):

$$\Delta P = C_P \tfrac{1}{2}\rho U^2 \geq (\rho-\rho_{air})gH \cong \rho gH, \tag{2}$$

where C_P, ρ, ρ_{air}, and g are the negative pressure coefficient of the hydrofoil, the density of water, the density of air, and the gravitational acceleration, respectively. Note that $\rho \gg \rho_{air}$. From Eq. (2), we can estimate the critical velocity for air entrainment $U=U_E$:

$$U_E \cong \sqrt{\frac{2gH}{C_P}}. \tag{3}$$

In this simple formula, C_P is not defined as a point wise value on the hydrofoil surface but is given by average value of local negative pressure coefficient distribution in the region between the hydrofoil and the outlet of air induction pipe (AIP). Thus, the WAIP is designed to provide strong negative pressure region between the hydrofoil and AIP so that the above-given critical velocity U_E is lowered as small as possible.

Fig. 2 shows an experiment that demonstrates the effect of the towing velocity on the air entrainment by the WAIP (Kumagai et al., 2010). When the towing velocity U was smaller than the

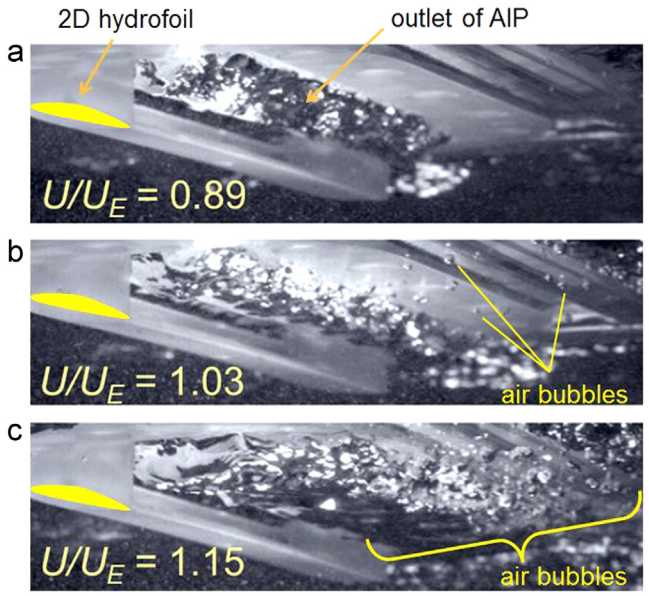

Fig. 2. Oblique upward views showing the thresholds for air entrainment by the WAIPs in towing tank experiments. The WAIP moves from right to left. (a) No air entrainment ($U<U_E$); (b) around the critical velocity U_E; (c) air entrainment and subsequent bubble formation ($U>U_E$).

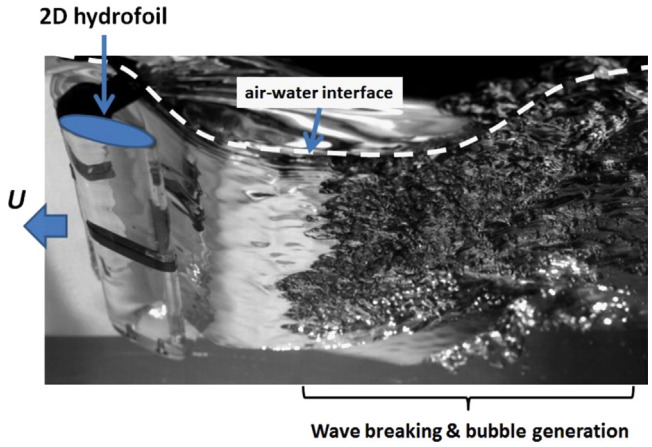

Fig. 3. Bubble generation by a moving hydrofoil (U=750 mm/s, θ=20°, chord length=50 mm, thickness=9.5 mm).

critical value U_E, no air entrainment was observed (Fig. 2a). Simple theory enabled prediction of the air entrainment threshold (Fig. 2b), and the volume of air bubbles increased with increasing towing velocity (Fig. 2c).

2.2. Power required for bubble generation

The air entrainment capacity of a hydrofoil depends on C_P: a higher C_P enables deeper release of the air at a given cruising velocity (Eq. (3)). However, the drag effect of the hydrofoil when installed on the ship's hull should also be considered when we discuss the net power saving performance for the ship.

As a first-order approach, we consider a hydrofoil moving at a constant velocity U under the water surface. The total power W necessary for air entrainment at an air-volume flow rate Q into the water can be described as

$$W = W_0 - W_L + W_D. \tag{4}$$

here, W_0 is the power required for air release at a water depth H, i.e.,

$$W_0 = \rho g H Q. \tag{5}$$

here we consider only the potential energy for air-blowing into water since WAIP system does not require air compression (see Eq. (1)). W_L in Eq. (4) is the power saved by the negative pressure generated above the hydrofoil, where

$$W_L = C_P \tfrac{1}{2} \rho U^2 Q, \tag{6}$$

and W_D is the power consumed in overcoming the drag force of the hydrofoil that is protruded from the ship's hull, where

$$W_D = C_D \tfrac{1}{2} \rho U^2 A, \tag{7}$$

where C_D and A are the drag coefficient and the projected area, respectively, of the adopted hydrofoil. From Eqs. (4)–(7), the total power W required for air induction into the water via the hydrofoil-supporting mechanism can be rewritten as

$$W = \rho B \left[g H \alpha U - \frac{1}{2} \left(C_P \alpha - \frac{A}{B} C_D \right) U^3 \right]. \tag{8}$$

here, the air volume flow rate is alternatively given by $Q=\alpha BU$, where α and B are the mean void fraction and the vertical cross-sectional area, respectively, of the air bubble-mixed layer over the ship's hull. Eq. (8) tells us that the power required for bubble release is saved by installing the hydrofoil when the following condition is satisfied;

$$C_P \alpha > \frac{A}{B} C_D \approx \frac{L}{h_b} C_D \sin\theta, \tag{9}$$

where L, h_b, and θ are the chord length of the hydrofoil, the air bubble-mixed layer thickness, and the angle of attack, respectively. The theory indicates that a hydrofoil with a high C_P/C_D ratio should be used to obtain high net power saving performance, which is the reason why we use hydrofoils rather than bluff bodies.

We should also note that Eq. (8) gives another critical velocity U_c at which the system reaches the power-free condition, $W=0$. This critical velocity is derived as below, and is always faster than the previous kind of critical velocity U_E.

$$U_c = \sqrt{\frac{2gH\alpha}{C_P\alpha - (L/h_b) C_D \sin\theta}}. \tag{10}$$

As an example, if we consider a NACA 65-410 hydrofoil (where C_P=1.50, C_D=0.015 at θ=10°) under conditions of H=2–5 m, α=5%, L=50 mm, and h_b=20 mm, then U_c=5.3–8.5 m/s. This simple estimate shows that both high-speed marine vehicles and moderate-speed marine vehicles can save the net power required for air release by installing the hydrofoil device.

3. Performance tests and scaling for total drag reduction by a hydrofoil device

In the previous section, we presented theory with regard to the air entrainment principle of the hydrofoil device. Here, we describe laboratory experiments to examine the process of bubble generation and its role in reducing the frictional drag of the downstream horizontal flat wall.

3.1. Hydrofoil device bubble generation process

Fig. 3 shows towing experiments on bubble generation by a moving hydrofoil close to an air–water interface. After the atmospheric air is entrained by the negative pressure, instability takes place on the air–water interface so that smooth interface naturally transits to turbulent state as seen by the dark area in the photograph. The transition occurs because of wave-breaking, i.e. upstream water which is accelerated by the hydrofoil's curvature to be faster than the gravitational wave propagation velocity dashes into the slow downstream water region. The wave breaking threshold is given by the wave steepness (the height/length ratio of a wave) and it was found to be approximately 0.1 (Kumagai et al., 2010, 2011a, 2011b). Beyond this threshold, small bubbles are naturally ventilated into a thin layer just beneath the original gas–liquid interface, and this phenomenon supports continuous but active release of small bubbles for the downstream region close to the wall. It is worth noting that this threshold is not a specific finding only for the WAIP system, but is known as a general trend of deep water wave-breaking mechanism reported such as in ocean wave breaking (Peregrine, 1983; Toffoli et al., 2010).

Small bubble generation observed behind the hydrofoil is interpreted as energy conversion from the wave energy to turbulent kinetic energy. Since the wave energy is produced by the rapid deflection of water flow above the hydrofoil, the design of the hydrofoil should be optimized to promote the wave-breaking. In its downstream, bubbles of various sizes are potentially generated because of a broad spectrum in wave number coming out on the turbulent interface. Among them, large bubbles are un-survivable in strong shear so that only small bubbles occupy the downstream turbulent boundary layer. The maximum survivable bubble size is scalable with the following Weber number We_f, which describes

the bubble deformability due to shear against surface tension:

$$We_f = \frac{\rho U^2 d}{\sigma} = \frac{\rho d}{\sigma}\left(\frac{dU}{dy}d\right)^2 \approx \frac{\rho d^3 U^2}{\sigma \delta^2}, \quad (11)$$

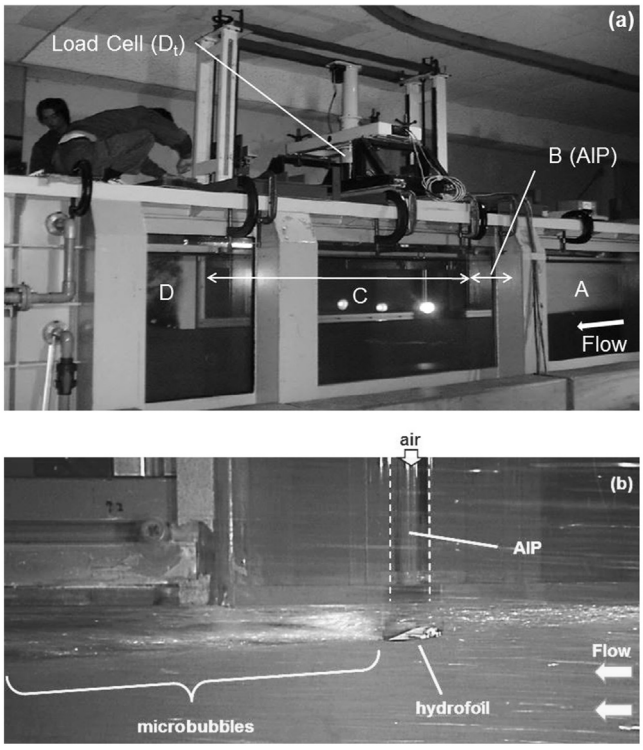

Fig. 4. (a) Circulating water channel (West Japan Fluid Engineering Laboratory Co. Ltd.); (b) microbubbles generated by the hydrofoil device.

where σ, dU/dy, and δ are the surface tension of the bubble, the shear rate around the bubble, and the turbulent boundary layer thickness, respectively. If we assume that the critical Weber number at which the bubbles break up is of the order of 10, the size of the air bubbles for a cruising speed U=5–10 m/s is expected to be around 200 to 300 μm.

3.2. Measurement of drag reduction by the hydrofoil device

The amount of drag reduction provided by the small bubbles depends on the void fraction, the bubble size, the flow conditions, and the position where the bubbles are generated. The internal fluid mechanics of bubble-base drag reduction contains a long and complex story as one of the authors recently reported in a review paper (Murai, 2014). We are not going into such physics hidden in bubbly two-phase turbulent boundary layer in the present paper, but we here examine for engineering purpose how much the small bubbles generated by our hydrofoil device reduce the drag of a flat plate downstream. Our experiments were carried out in a circulating water channel as its look is shown in Fig. 4. The flow velocity of the circulating water (V) was set at 5.6 m/s, considering the typical cruising velocity of ships. In the test section, four kinds of measurement instruments are setup as listed in Table 1. The experimental model ship was designed to focus on the WAIP performance test, and it consists of four parts as shown by A, B, C, and D in Fig. 5. The total drag force acting on parts B and C (D_t) was measured by a single load cell. In parallel, the drag force acting on part B was separately measured by another load cell (D_o). Hence the drag force acting on the flat acrylic plate of 2.6 m long (D_b) was given by

$$D_b = D_t - D_o. \quad (12)$$

Table 1
Specifications of measuring instruments.

Item	Instrument	Specifications
Flow velocity	Pitot tube Differential pressure cell	3.0 mmϕ Capacity: 0.2 kgf/cm^2
Induced air volume	Propeller type velocity meter	Propeller Dia.: 3 mm, Max. velocity: 2.0 m/s, nonlinearity: ±2.0% F.S.
Drag on box of 2.6 m long	Load cell (strain gauge type)	Rated load: 500 N, nonlinearity: ±0.1% F.S.
Drag on box of 0.25 m long	Load cell (strain gauge type)	Rated load: 100 N, nonlinearity: ±0.3% F.S.
Static pressure	Tube Differential pressure cell	3.0 mmϕ Capacity: 0.1 kgf/cm^2

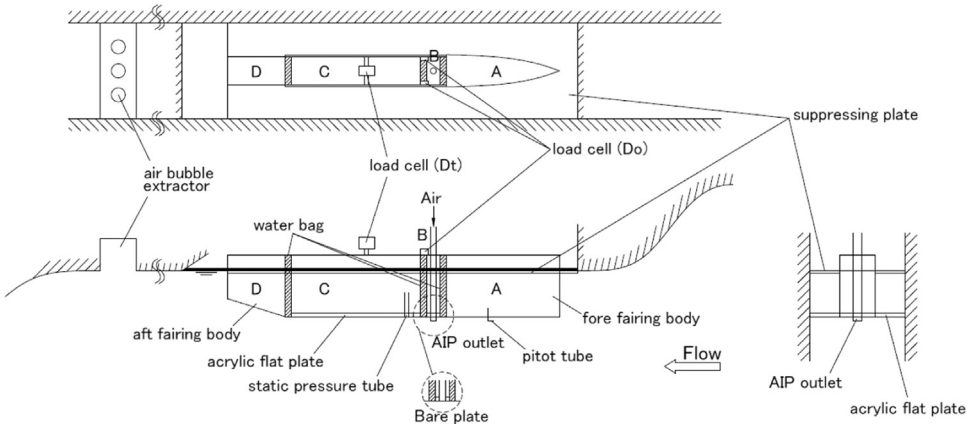

Fig. 5. Schematic diagram of the experimental set-up: Top view (upper), side view (lower), and front view (bottom right).

The volume flow rate of air entrainment by the hydrofoil (Q) was also monitored using a propeller-type flow meter attached to the AIP (air induction pipe). The hydrofoil that we employed in the device was an NACA 65_3-618 hydrofoil, which was attached to the bottom of the AIP. This position is hereafter defined as origin, $x=0$ to evaluate the streamwise persistency of drag reduction. We examined three angles of attack: $\theta=12^\circ$, 16°, and 20° together with the drag force measurement for a bare plate (D_0) as a reference (i.e. the case without a hydrofoil).

Table 2 summarizes our experimental results. Here, the increase in drag force caused by the attachment of the hydrofoil, ΔD_0, is

$$\Delta D_0 = D_0(hydrofoil) - D_0(bare\ \ plate), \tag{13}$$

where $D_0(hydrofoil)$ and $D_0(bare\ plate)$ are the drag forces with and without the hydrofoil, respectively. $\Delta R_{2.6m}$ is the drag reduction for the flat plate (part C) caused by the air bubbles that were generated by the hydrofoils:

$$\Delta R_{2.6m} = D_b(hydrofoil) - D_b(bare\ \ plate). \tag{14}$$

As shown in Table 2, we confirmed that the drag reduction ($\Delta R<0$) on the flat plate of part C was caused by the air bubbles generated by the hydrofoil device. From the specifications of two load cells applied for Eqs. (13) and (14), measurement uncertainty for ΔD_0 is estimated to be 0.7%, and that for $\Delta R_{2.6m}$ is 1.2%.

3.3. Estimation of total drag forces for a full-size ship

In the previous section, some readers may have supposed that attachment of the hydrofoil causes increased drag because the magnitude of ΔR is smaller than that of ΔD_0. However, the 2.6 m flat plate (part C; from $x=2.216$ m to 4.816 m) considered in the previous experiment corresponds only to a small part of a real ship's hull which is typically longer than 10 m. In this section, we describe the total drag force F_{total} that acts on a long flat plate for application to full-size ships.

For practical use, we simply express the total drag force F_{total} that is acting on a flat plate with length L by use of local friction factors with and without the air bubbles, represented by C_f and C_{f0}, respectively:

$$F_{total} = D_t - \int_0^L \frac{1}{2}\rho V^2 C_{f_0}\left(1-\frac{C_f}{C_{f_0}}\right) B_h\ dx. \tag{15}$$

here, B_h is the horizontal width of the bubble-mixed layer. The second term on the right hand side of Eq. (15) can be rewritten using $\Delta R_{2.6m}$ as follows:

$$\Delta R_{total} = -\int_0^{2.216m} \frac{1}{2}\rho V^2 C_{f_0}\left(1-\frac{C_f}{C_{f_0}}\right) B_h\ dx + \Delta R_{2.6m} - \int_{4.816m}^{L} \frac{1}{2}\rho V^2 C_{f_0}\left(1-\frac{C_f}{C_{f_0}}\right) B_h\ dx, \tag{16}$$

where

$$\Delta R_{2.6m} = -\int_{2.216m}^{4.816m} \frac{1}{2}\rho V^2 C_{f_0}\left(1-\frac{C_f}{C_{f_0}}\right) B_h\ dx. \tag{17}$$

Although the magnitude of $\Delta R_{2.6m}$ is smaller than that of ΔD_0 in the previous experiments (Table 2), the total drag reduction due to the air bubbles ΔR_{total} overcomes the increase in drag caused by the hydrofoil attachment (ΔD_0) if the plate length L is sufficiently

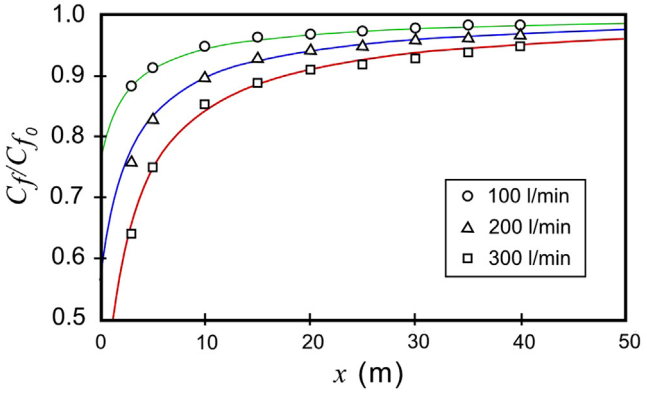

Fig. 6. Local skin friction ratio (C_f/C_{f0}) as a function of distance x. The plots are made from IHI experimental data (Watanabe et al., 1998). The fitting curves were obtained by regression analysis (see text).

Table 3
Curve fittings of Eq. (18) obtained from the drag measurements of a slender ship model of 40 m length (Watanabe et al., 1998).

Gas-volume flow rate Q (l/min)	Impact distance a (m)	Approach distance b (m)
100	0.7	2.9
200	1.3	2.9
300	2.0	2.9

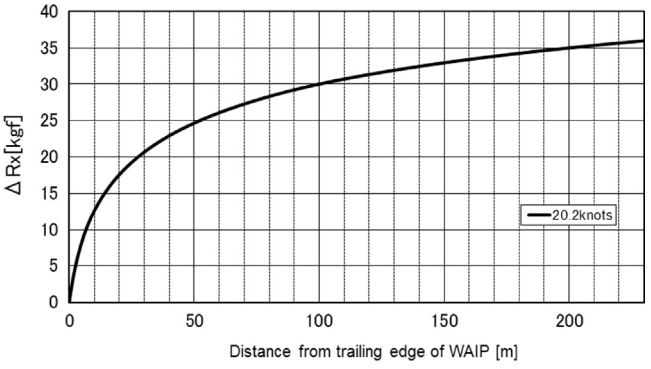

Fig. 7. Drag reduction produced on a flat plate by a hydrofoil device, $\Delta R_x = \Delta R_{\text{total}}$, as a function of distance x from the trailing edge of the WAIP.

Table 2
Experimental results on the effect of hydrofoils on drag forces.

Type	Attack angle (deg)	V (m/s)	D_t (kgf)	D_o (kgf)	D_b (kgf)	ΔD_o (kgf)	$\Delta R_{2.6m}$ (kgf)	P_s (mAq)	V_{air} (m/s)	Q (m^3/mi.)	X_c (m)
Bare plate			19.7	1.2	18.5			0.010			
NACA12	12	5.6	20.9	3.8	17.1	2.6	−1.5	−0.044	0.110	0.035	8.5
NACA16	16	5.6	21.6	4.6	17.0	3.4	−1.5	−0.210	0.140	0.044	11
NACA20	20	5.6	22.6	6.0	16.6	4.8	−2.0	−0.307	0.135	0.042	12

large. Here, we define the compensation distance X_c as the distance where $\Delta D_0 = \Delta R_{\text{total}}$. To apply our device to a real ship, we should use a hydrofoil with a shorter X_c. The experimental results indicate that "NACA12" (i.e. the NACA 65_3-618 with the angle of attack $\theta = 12^\circ$) is the best hydrofoil for reduction of the drag of ships in the tested range ($X_c = 8.5$ m, Table 2).

3.4. Estimation of local skin friction ratio and total drag reduction by a hydrofoil device

To estimate ΔR_{total} for full-scale ships, it is necessary to know the local friction factor C_f/C_{f0} as a function of the distance from the air release point, x. We referred to experimental drag reduction results for a long, slender ship model ($L = 40$ m, $B = 0.6$ m) in a towing tank (Watanabe et al., 1998). The calibration curves of C_f/C_{f0} as a function of x are obtained using the following equation:

$$\left(\frac{C_f}{C_{f_0}}\right) = 1 - \frac{a}{x+b}, \tag{18}$$

where a and b are constants determined by curve fitting based on a least-squares regression (Fig. 6, Table 3). Because these constants have length dimensions, we call a and b the impact distance and the approach distance, respectively. The approach distance b seems to be independent of the gas volume flow rate Q, whereas the impact distance a depends on Q. If we assume that $a = 0$ when $Q = 0$, then we obtain the following empirical equation:

$$a = (3.96 \times 10^2)Q. \tag{19}$$

Note that the impact distance a and the gas volume flow rate Q are given by the units of m and m^3/s, respectively.

If we apply the relationship of Eq. (19) to the gas volume flow rate realized in a hydrofoil when using the experimental constraints of the partial drag reduction $\Delta R_{2.6m}$ (Eq. (17)), the total drag reduction provided by the hydrofoil device, ΔR_{total}, as a function of x is obtained from Eq. (16). Fig. 7 shows ΔR_{total} when we use the local skin friction formula derived by Schlichting (1979):

$$C_{f_0} = \left[2\log_{10}(\mathrm{Re}_x) - 0.65\right]^{-2.3}. \tag{20}$$

The Reynolds number Re_x is defined as

$$Re_x \equiv \frac{Vx}{\nu}, \tag{21}$$

where ν is the kinematic viscosity of the fluid (water at 15 °C). For a long flat plate, while the local drag reduction ratio decreases with increasing x because of bubble diffusion, the total drag reduction integrated in the streamwise direction increases with increasing x.

3.5. Air bubble release method for drag reduction

To reduce the drag on a ship's hull at 15–20 knot, the injection of small bubbles (< 0.5 mm) into the turbulent boundary layer is desirable, because only an adequate supply of these small bubbles can markedly reduce the turbulent momentum transfer, i.e., the skin friction of the wall. Although the mechanism of the drag reduction produced by such small bubbles remains an open question academically, the current common understanding from historical experimental observations is that the injection of these small bubbles into the turbulent region causes reduction of the Reynolds shear stress (Kitagawa et al., 2005). This implies that the ideal condition is to have the highest bubble number density at the peak Reynolds shear stress position, which is located between the viscous sublayer and the buffer layer of the turbulent boundary layer (Murai, 2014). Additionally, small bubbles tend to be accumulated naturally into the turbulent shear layer, as reported in previous studies of bubbly two-phase jets and also for hydrofoil (Ohashi et al., 1990). To be precise, small bubbles tend to remain in a high-enstrophy region where the second invariant of the velocity gradient tensor has a negative value (Kitagawa et al., 2001). In the flow beneath a moving ship, this region corresponds to the layer with the most active turbulent eddies, and thus the small bubbles remain for a long period inside the turbulent boundary layer and resist the turbulent diffusion effect.

For provision of a supply of these small bubbles to the turbulent boundary layer, the method of air injection is highly important. Fig. 8 shows an illustrative comparison how the present WAIP system should be operated. When the ship's draught is shallow (< 5 m), the hydrofoil works as a self-priming pump, as discussed in Section 2. As a result, the small air bubbles are released near the ship's hull by the hydrofoil device. For larger vessels with deeper draughts (> 5 m), the pressure reduction by the hydrofoil is insufficient and a moderate air pressure rise is required to maintain bubble generation. In this case, the air–water interface should be placed between the AIP outlet and the top surface of the hydrofoil (Fig. 8a). Otherwise, for example, if we use blowers with high air volume flow rates, the upper surface of the hydrofoil would be covered with air cavities (Fig. 8b), and it would no longer be able to work as an air inducer using the pressure lowering effect of the hydrofoil. On this condition, the hydrofoil's own drag would be highly increased because of different phase (gas/liquid) between the top and the bottom surfaces. Further increases in the air-volume flow rate using blowers would leave the hydrofoil completely isolated from the ambient water flow (Fig. 8c), and only large bubbles would be produced outside the boundary layer. Moreover the hydrofoils would work as a resistance of the air injection by blowers. We must avoid such situations, which are simply a waste of bubble generation energy. Therefore the pressure regulator from the air reservoir of the compressor, instead of the blower, is necessary for the WAIP system to control the position of the air–water interface above the hydrofoil.

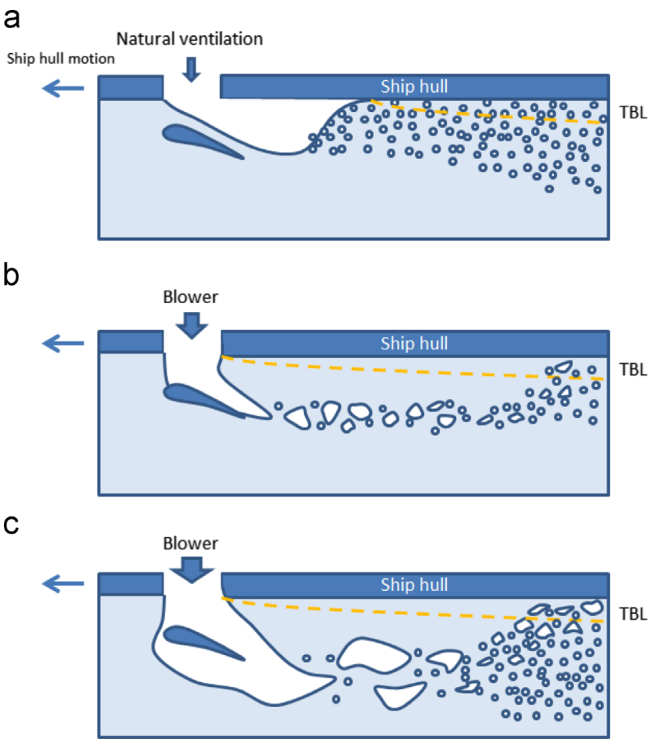

Fig. 8. Methods of air supply over a ship's hull: (a) WAIP with natural ventilation; (b) WAIP with blower (where the hydrofoil is useless as a self-priming pump); (c) WAIP with blower (air flow is too high).

Table 4
Summary of actual sea trials with WAIP.

Ship name	Adventure2	Santander Ferry 1	New Ferry Misaki	Filia Ariea
Ship type	Fishing boat	150 Persons passenger	Roll-on/roll-off Cargo	Long hold Cargo
Sea trial date	July 2002	October 2004	August 2005/2006	July 2008
Weather condition	Fine	Fine	All sailable weather	Fine
Test place	Imari bay, Japan	Cebu, Philippines	Nagasaki, Japan	Neatherland
Principal dimensions (m) Lpp × Bmld × Dmld × Output	12.62 × 2.2 × 0.83 × 500 ps x1	28.8 × 5.45 × 1.55 × 350 ps x2	68 × 12.3 × 9.9 × 1500 ps x2	84.95 × 13.75 × 5.55 × 1440 kw x1
Number of installed WAIP	2 (Single activated)	10 (4 in front, 6 in rear)	14 and 34	52 (34 submerged)
Remarks	The first sea trial for WAIP installed ship. Performance prooved. Calculation method established	Plural WAIPs installation for a ship prooved	Compressor assisted WAIP installed. 2.2 kw × 2 compressors, with 0.4 kg G/cm^2 set. at pressure regulator.	By mistake, blowers installed, then cut off and natural ventilation WAIP tested with 34 WAIPs underwater
Net drag reduction	4% by 1 WAIP.	16% by 10 WAIPs	6% by 14 WAIPs 9% by 34 WAIPs	10% by 34 WAIPs
Measurement system	Flowmeter	Flowmeter	Over 140 days refueled, average	Brake horse power measurement and speedmeter

4. Applications to various ships

In the previous sections, our semi-theoretical estimations have predicted that significant drag reduction can be obtained by the installation of hydrofoil devices (i.e. WAIPs) on a long flat plate. Here, we report the actual application of these devices to four ships. The specifications and examination conditions of these sea trials are briefly summarized in Table 4. Basically the same WAIP systems (Fig. 1) were installed on all the four kinds of ships. However, we should note that each examination was conducted in different operation schemes due to various restrictions in sea trials. As inevitable fact, our data to be shown hereafter involve various uncontrollable factors such as data-sampling method allowed in each ship and meteorological variances. Therefore, consequent drag reduction performance was evaluated upon largely fluctuating nature. In this section, we will review each of the sea trials with describing the examination scheme in detail so that how the WAIP system worked on actual sea is demonstrated.

4.1. Adventure 2

In December 2002, we installed two hydrofoils beneath a small fishing boat Adventure 2 (Fig. 9a) as historically the first feasibility test of the WAIP system. Two WAIPs were located in-line to the main stream and the downstream one was activated. The flow conditions beneath the ship were monitored through a window located downstream of the WAIPs (Fig. 9b). As the ship's speed increased, the atmospheric air was entrained into the seawater as we expected, and the generation of small bubbles was confirmed at the downstream as it look white cloud in the window (see Fig. 9c).

Fig. 9d shows the fuel consumption rate as a function of the ship's speed. The power saving effect depends on the ship's speed, and a fuel saving of about 4% was provided by the device when the ship's speed was approximately 29 knot. The amount of drag reduction was modest because we installed only two WAIPs in order to evaluate the sensitivity of the WAIP-to-drag reduction performance. Supplementation on the examination scheme is given below.

The comparison of fuel consumption rate between "with WAIP" and "without WAIP" for Adventure 2 was conducted in a few hours (from 10AM to 2PM) of a single day. It was a fine day with calm wind (wind speed < 5 m/s) without sudden climate change, judged suitable for testing. The route for the examination was 10-sea mile round-trips in Imari Bay, Nagasaki, Japan at five different log speeds. Inside this bay, local maximum seawater current was estimated to be 1.0 m/s. Each single plot of the fuel consumption rate in Fig. 9 is the time averaged value for 10 min. Since the ship hull was made of FRP, we mounted resin-made hydrofoils which were easily removable in a short working time for returning to the original flat surface by capping the air induction pipes. This allowed us to measure the differential fuel consumption rate provided by WAIP's function appropriately. Thus, the drag increment due to the protrusive hydrofoil was excluded in the case of "without WAIP" in Fig. 9(d). In combination of the above-mentioned conditions, the measurement uncertainty of fuel consumption rate due to fluctuating seawater current is estimated to be 2.8%, and that due to wind is 1.8%. Therefore, total measurement uncertainty is estimated to be 3.3%. This value is not small enough to the measured fuel saving ratio about 4%, and we thereby declare that the significance of measurement result is not fully guaranteed. This is simply reasoned by only a single operation of the WAIP system which covers the ship with bubbles at less than 10% of the total wet-surface of the hull as shown in Fig. 9(b). Adventure 2 is positioned as our first feasibility study and this led to the application to larger ships to investigate the more integral performance of the WAIP system as described below.

4.2. Santander Ferry I

The second sea trial was for a ferry boat of 28.8 m-long, named Santander Ferry I (Fig. 10a). Ten WAIPs were installed on the ship's hull (Fig. 10b) and the ship cruised at approximately 12 knot. We conducted the WAIP performance tests twice for the ferry in September 2004 and February 2005. The location of both sea trials was the route between Santander (Cebu Island) and Dumaguete (Negros Island) in Philippine, and these tests were carried out during commercial use with boarding of passengers. From the first test in September 2004, we confirmed about 10% of fuel saving in gross average, and based on it we proceeded to the second test in February 2005 which was carried out with recording various parameters.

Table 5 shows experimental results of the second test. The WAIP operation conditions were classified to four cases as shown in the rows. "All closed" means that all the air induction pipes (AIP) were closed by valves so that bubble injection stops. "No.1" and "No.2" mean the valve conditions for front four WAIPs and rear six WAIPs, respectively. Fuel consumption rate over 500 s was recorded as the

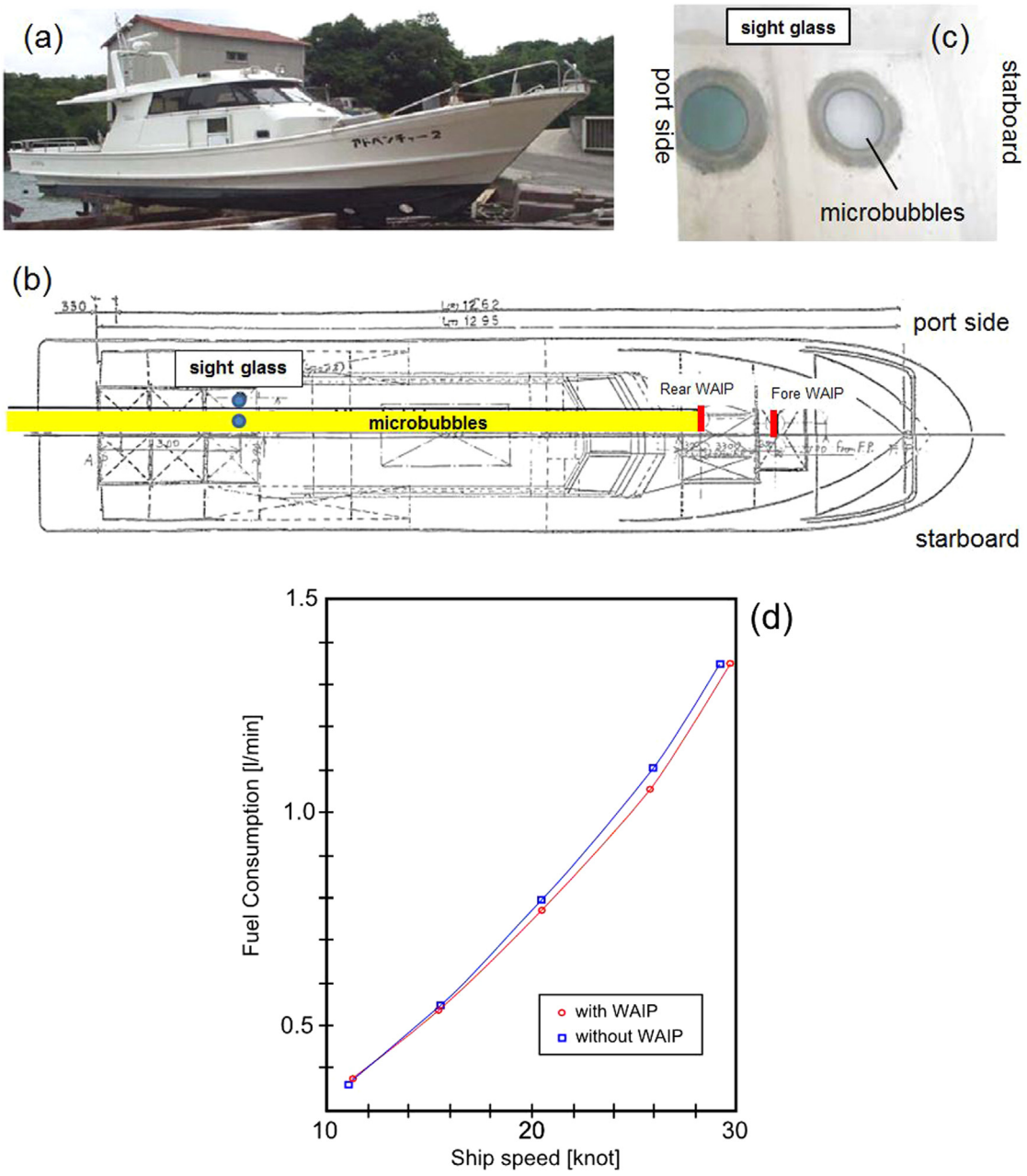

Fig. 9. Full-size ship test on the Adventure 2: (a) photograph of the adventure 2 (12.62 m (length between perpendiculars, Lpp), 2.7 m (beam molded, Bmd), 0.83 m (depth molded, Dmd), 500 ps (power)); (b) arrangement of the hydrofoil device; (c) bubble clouds (white) were observed in the right-hand window; (d) fuel consumption results for the ship with (red curve) and without the device (blue curve). (For interpretation of the references to color in this figure legend, the reader is referred to the web version of this article.)

ferry cruised a periodical round trip "Go" and "Back" four times a day. Since there was a large variation in the fuel consumption rate because of change in the number of passengers and so on, we show the weight-corrected fuel consumption rate in the table. Furthermore, the influence of speed difference has been corrected to obtain the comparable values that are shown on the bottom line of the table. From this, we confirmed 16% reduction in the fuel consumption rate as all the ten WAIPs were activated ($16\% = 100 \times (91.0 - 76.5)/91.0$). The data in the case "No.1 only open" corresponds to 21% reduction, and implies that bubble injection from the front part of the ship is more effective. However, the authors still suspect that this value is too large to believe. The measurement uncertainty of fuel flow rate, total weight, and ship speed are estimated to be less than 3%. In contrast, fuel consumption dependence on sea and wind states would be more effective. To clarify this issue in the success of a single-day sea trial, we advanced to the next sea trial spending more than 100 days for guaranteeing statistics reliability as reported next.

4.3. New Ferry Misaki

As the third application of the WAIP system, we chose a 68 m-long cargo, called New Ferry Misaki. Fig. 11 shows a photograph of the ship, and it cruises at about 18 knot on sea. Since New Ferry Misaki is much larger than previous test cases, we installed 34 WAIPs. Another feature is that we introduced compressors to assist the WAIP system because of the deep draught. As explained in Section 3.5, the additional pressure should be adjusted not to

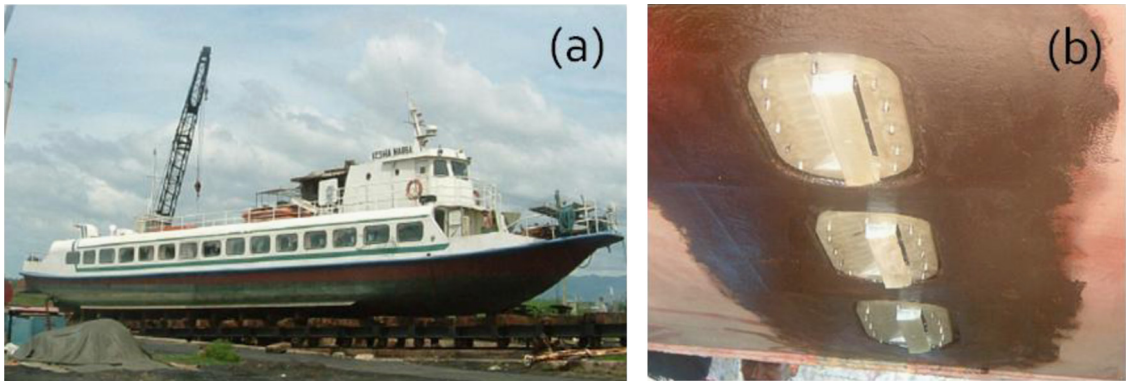

Fig. 10. (a) Santander Ferry I (28.8 m (Lpp), 5.45 m (Bmd), 1.55 m (Dmd), 350 ps × 2 engines); (b) rigging with the WAIPs (the seawater flows from right to left).

Table 5
Fuel consumption rate of Santander Ferry.

Santander Ferry	WAIP operation conditions							
Starboard side engine	All closed		No.2 only open		No.1 only open		All open	
	Go	Back	Go	Back	Go	Back	Go	Back
Date 19th Feb 2005 time	7:41–8:15	9:01–9:35	10:28–10:59	11:56–12:29	13:30–14:03	15:08–15:42	16:35–17:10	18:04–18:35
Weather/sea state	Fine/calm	Fine/calm	Fine/calm	Fine/calm	Fine/W.waves	Fine/W.waves	Fine/W.waves	Fine/calm
Elapsed time [s]	550	534	537	513	545	517	517	543
Total variable weight [t]	3.776	4.231	4.946	3.126	2.801	3.191	2.866	3.451
Fuel remained on board	1.566	1.501	1.436	1.371	1.306	1.241	1.176	1.111
Persons including passengers	2.210	2.730	3.510	1.755	1.495	1.950	1.690	2.340
Speed measured [knot]	11.455	11.798	11.732	12.281	11.560	12.186	12.186	11.602
Fuel consumption rate [l/h]	101.1	80.5	79.6	72.6	72.2	66.4	77.2	70.9
Weight corrected with 3.776 [t]								
Speed [knot]		11.817	11.780	12.252	11.519	12.160	12.146	11.589
Fuel consumption rate [l/h]		80.9	80.6	72.1	71.5	66.0	76.5	70.7
Averaged fuel con. rate [l/h]	91.0		80.6		71.5		76.5	

Fig. 11. New Ferry Misaki (68.0 m (Lpp), 12.3 m (Bmd), 8.95 m (Dmd), 3.2 m (draft), 4076 ps (power)). (Courtesy of Hirofumi Morieda).

lose the original performance of the hydrofoil. The pressure rise adopted to AIP was 41 kPa using pressure adjusting valves, which corresponds to hydrostatic pressure of 4 m. This adjustment helps the water surface in the AIP with reaching the region above the hydrofoil. New Ferry Misaki has been navigating in the route called Shimo-Gotou Route; Nagasaki New Port–Fukue–Naru–Wakamatsujima. She has made one round trip a day with single refueling. Weather and wave condition were not recoded but at least she was operated under commercially operable states for shipping service. She cruised 77 days without air injection to be without WAIP, and 148 days with WAIP operation. The fuel consumption rate for her engine has been reported to the authors from chief engineer's log book. It is noted that the total fuel consumption is about 15 to 20% larger than that for main engine because of ship-interior uses. It is irrelevant to drag reduction phenomenon and was not considered.

Table 6 shows the records of daily fuel consumptions for her main engine without WAIP, which were taken in October 2004 to August 2005. The average daily fuel consumption for 77 operation days was 4106 l/day with a standard deviation of 480 l/day (11.6% to the average). This large deviation originates from daily variances both in weather and shipping load. From the inverse square root law of average-sampling theory, true average exists in the range from 4051 to 4161 l/day. Table 7 shows the same records with 34 WAIPs installation. The data were acquired in 148 days, and the

Table 6
Main engine fuel consumption of New Ferry Misaki without WAIP.

Date	Oct-04	Feb-05	Mar-05	Apr-05	Jul-05	Aug-05	
1						4,687	
2						4,867	
3						4,647	
4						4,767	
5						4,657	
6						3,887	
7		4,017				3,897	
8		3,887				4,657	
9		3,857				4,587	
10		4,217				4,727	
11		3,237				4,737	
12		3,717	4,197			4,677	
13		3,047	3,247			4,597	
14	3,907	3,937	3,887			3,817	
15	3,817	4,847	3,777			3,897	
16	3,747	4,247	3,897			4,387	
17	2,867	4,207	4,607			4,387	
18	3,627	4,297	4,267			4,417	
19	4,887	3,927	3,857	3,867		4,427	
20		3,927	3,017	3,847		4,847	
21	4,587	3,977	3,077	4,267		3,967	
22	3,897	4,027	4,547	3,947		4,477	
23	3,817	4,147	4,107	3,907			
24	2,987	4,207					
25	3,807	4,037					
26	4,177	4,097					
27		3,607			4,407		
28					4,557		
29					4,797		
30					4,677		
31					3,787		Grand total
Sum	46,125	83,469	46,485	19,836	22,226	98,016	316,157
Days	12	21	12	5	5	22	77
Average	3,844	3,975	3,874	3,967	4,445	4,455	4,106

average daily fuel consumption decreases to 3733 with a standard deviation of 191 l/day (5.1% to the average). The true average estimated from the sampling theory exists in the range from 3717 to 3749 l/day. Thus, the influence of 34 WAIPs installation to average daily fuel consumption is concluded to be sufficiently significant. The resultant fuel saving of the main engine was 9.1%. Another sea trial for the same ship with 14 WAIPs installation, which were carried out in 2004, obtained 5.8% reduction in fuel consumption rate. This value is reasonable since drag reduction effect is expected monotonically obtainable to the number of WAIPs. This trend is shown in Fig. 12. Here the fuel consumption rate for zero-WAIP condition includes additional fuel use for ship drag increment due to many hydrofoils. However, the additional drag is estimated to be only 110 kgf, which is less than 1% of the total drag of the hull. As explained in Section 3.3, the WAIP's function overshadows their own drag as those are applied in large facilities.

4.4. Filia Ariea

The forth sea trial was for a 85 m-long coaster, named Filia Ariea in July 2008. Fig. 13 shows a photograph of the side surface of the Filia Ariea where open holes were being provided to connect WAIPs in a dock. Total number of WAIPs installed on this ship was 52, among which 34 WAIPS were submerged in sea because of her draught was shallow (2.5 m, mean). Two blowers of 2.2 kW were mounted to the WAIP to see the influence of additional air supply to the natural ventilation although it was unnecessary in her original design. Measurements of the ship's speed and maneuvering were carried out by Belkoned Marine Service b.v. (Belkoned Marine Service b.v., 2008) according to ISO 15016: 2002 (Guidelines for the assessment of speed and power performance by analysis of speed trial data). Unfortunately, the legend of the original figure given on page 9 of the Belkoned Report (2008) contains an error, which led to a misunderstanding of the results. Fig. 14 shows a revised version of the results provided by Belkoned (2012, page 9A). In the revised figure, the red diamonds indicate the results of natural ventilation for the Filia Ariea with WAIPs, but without use of blowers. In contrast, the blue triangles are the shaft power of the Filia Ariea's sister ship, the Filia Nettie, which operated without the WAIP system. As these two lines clearly indicate, the power savings increased as the ship's speed increased, and a power-saving ratio of about 10% was achieved. These two ships are exactly the same in geometry, engines, interior structures, and surface coating except installation of WAIPs. Only aging of the ship may cause their mutual difference after their launching in different years, but which cannot be considered as a factor of 10% to change. The green circle at the speed of 14.2 knot indicates the case of Filia Ariea where a blower for surplus air supply was connected to the WAIPs but was not working. This is the same as natural ventilating operation of WAIPs. The cross indicates the result when the blower was working at 50% of its full power, and it is located slightly higher than the red curve fitted for three red diamonds. From this blowing condition, we infer that too much air was forcibly injected into the WAIPs so that the WAIP failed to release small bubbles in desired position, as explained in Section 3.5. For earning proper WAIP performance, we should again place a special emphasis with that only a moderate air pressurization keeps the air–water interface just above the hydrofoil so that the water and the air behaves smooth confluence above the hydrofoil to generate small bubbles in the downstream region.

5. Conclusions

We developed a device to be used as an air-bubble generator for drag reduction ships; the device consists of an air induction pipe (AIP) and an angled hydrofoil, and is called the winged air induction pipe, or WAIP. Air bubbles are released from the induction pipe outlet into the turbulent boundary of ship hull via the negative pressure produced above the hydrofoil beneath the AIP. In this paper, the theoretical principle of air entrainment by this device was described and its performance was confirmed by a series of laboratory experiments. A simple theoretical analysis for critical velocity at which air bubbles start to release was in good agreement to the observation in a towing tank experiment. To estimate the net drag reduction obtained by installing a single set of WAIP system, a circulating water channel experiment was carried out. From semi-empirical scaling, a compensation distance at which drag reduction exceeds the drag increment due to hydrofoil's own drag has been estimated to be less than 10 m at typical cruising speed.

Four kinds of full-scale tests were carried out to demonstrate the feasibility of the WAIP system while individual tests were conducted in different schemes owing to various restrictions in their sea trials. For a small fishing boat Adventure 2, single WAIP operation earned 4% of fuel saving but it was not fully guaranteed as we consider fluctuating nature in sea states. A passenger ferry Santander Ferry employed 10 WAIPs and obtained 16% of fuel saving for four round trips a day. In order to obtain higher statistic reliability in long operation, we advanced to 148-day sea trials using a long cargo New Ferry Misaki where 34 WAIPs were installed. She obtained 9% reduction in main engine fuel oil consumption in her commercial shipping service, by which fuel oil of 55,204 l was saved in 148 servicing days. In the case of

Table 7
Main engine fuel consumption of New Ferry Misaki with 34 WAIPs.

Date	Sep-06	Oct-06	Nov-06	Dec-06	Jan-07	Feb-07	Mar-07	
1			3,720	3,690		3,740	3,840	
2		3,740	3,660			3,780	3,790	
3		3,770	3,640			3,770	3,670	
4	3,760	3,750	3,550		3,740			
5	3,880	4,030		3,570	3,600	3,580	4,210	
6	3,870	4,110	3,620	3,520	3,730			
7	3,700	3,840	3,680	3,730		3,780	3,830	
8	3,710		3,580	3,730		3,720		
9	3,590		3,770		3,540	3,750	3,670	
10	3,280	3,570	3,650		3,630	3,660	3,730	
11	3,810	3,660	3,720	3,720	3,610			
12	3,710	3,560		3,700	3,740		3,740	
13	3,730	3,770	3,820	3,730	3,670	3,720	3,800	
14	3,830	3,650	3,820	3,650			3,710	
15	3,770		3,690	3,670		3,900		
16	4,900	3,610	3,850		3,650	3,700	3,780	
17		3,670	3,660		3,660		3,690	
18		3,680			3,770			
19	3,690	3,710			3,610	3,620	3,690	
20	3,580	3,700					3,730	
21	3,740	3,700	3,830			3,710		
22	3,790		3,760		3,590	3,700	3,700	
23	3,270	3,750			3,620	3,690	3,710	
24	3,210	3,820	3,860		3,510	3,670	4,870	
25	3,720	3,710		3,730				
26	3,570	3,600		3,650	3,760	3,690	3,910	
27	3,730	3,670		3,820	3,690	3,660	3,840	
28	3,680	3,590	3,750	3,930		4,030	3,830	
29	3,670		3,840	3,810	3,620		4,070	
30	3,680	3,500	3,720	3,650			4,010	
31		3,670			3,640		4,180	Grand Total
Sum	92,870	92,830	78,190	59,300	69,380	70,870	89,000	552,440
Days	25	25	21	16	19	19	23	148
Average	3,715	3,713	3,723	3,706	3,652	3,730	3,870	3,733

Unit of fuel consumption rate: l/day.

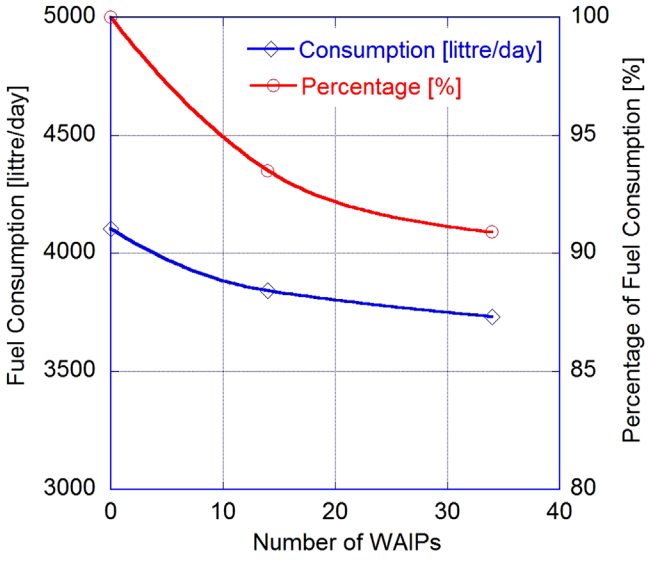

Fig. 12. Fuel consumption as a function of the number of WAIPs.

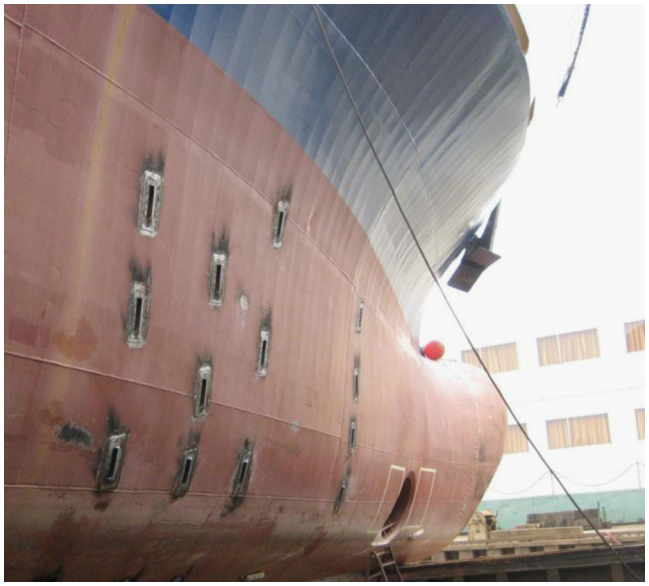

Fig. 13. Side view of the Filia Ariea (84.95 m (Lpp), 13.75 m (Bmd), 5.55 m (Dmd), 1440 kW (power)). WAIPs were installed on the ship as shown. (From Murai et al., 2010).

a long hold cargo Filia Ariea, 34 WAIPs out of a total of 52 were under water, and a net power saving of about 10% was achieved. As we experienced in large vessels with deeper draughts, the WAIP requires the assistance of an air compressor since the negative pressure provided above the hydrofoil fails in insufficient for realizing natural ventilation (see Eq. (2)). To the contrary, surplus air supply from blowers into air induction pipe alters the two-phase flow structure around the hydrofoil to totally lose the hydrofoil performance. For satisfactory operation of the WAIP system in ships with deeper draughts, future

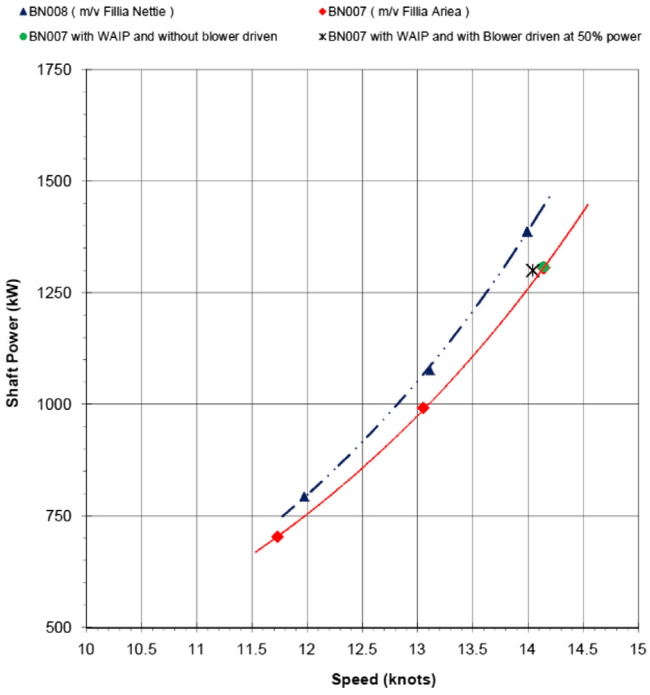

Fig. 14. Shaft power as a function of ship's speed (from the revised results given in the report by Belkoned, 2012 (page 9A)). The draught is 2.5 m (mean). (For interpretation of the references to color in this figure legend, the reader is referred to the web version of this article.)

studies will be conducted on (1) the optimization of the hydrofoils (e.g., the attachment of flaps, and hydrofoils suitable for two-phase flow) to enhance the hydrofoil's air entrainment performance, (2) appropriate operation of the air compressors to assist the device, and (3) investigation of their relevance to the downstream physics of the drag reduction.

Acknowledgments

The authors would like to thank Dr. Yuji Tasaka and Dr. Yoshihiko Oishi for their contributions to the WAIP project. This work was supported by the New Energy and Industrial Technology Development Organization (NEDO) of Japan (Grant no. 08 B 36002) and by JSPS KAKENHI (Grant no. 24236033).

References

Belkoned Marine Service b.v., 2008. Report No. 973-A/08, 2008.
Belkoned Marine Service b.v., 2012. Revised Version of the Report Page 9A, No. 973-A/08, 2008.
Ceccio, S.L., 2010. Friction drag reduction of external flows with bubble and gas injection. Annu. Rev. Fluid Mech. 42, 183–203.
Duncan, J.H., 1983. The breaking and non-breaking wave resistance of a two-dimensional hydrofoil. J. Fluid Mech. 126, 507–520.
Jang, J., Choi, S.-H., Ahn, S.-M., Kim, B., Seo, J.-S., 2014. Experimental investigation of frictional resistance reduction with air layer on the hull bottom of a ship. Int. J. Naval Archit. Ocean Eng. 6, 363–379.
Kitagawa, A., Murai., Y., Yamamoto., F., 2001. Two-way coupling of Eulerian–Lagrangian model for dispersed multiphase flows using filtering functions. Int. J. Multiphase Flow 27, 2129–2153.
Kitagawa, A., Hishida, K., Kodama, Y., 2005. Flow structure of microbubble-laden turbulent channel flow measured by PIV combined with the shadow image technique. Exp. Fluids 38, 466–475.
Kodama, et al., 2008. A full-scale air lubrication experiment using a large cement carrier for energy saving (Result and Analysis). In: Proc. Japan Soc. Naval Architects and Ocean Engineers Conference 6, pp. 163–166, 2008-05.
Kumagai, I., Nakamura, N., Murai, Y., Tasaka, Y., Takeda, Y., 2010. A new power-saving device for air bubble generation: hydrofoil air pump for ship drag reduction. In: Proc. Int. Conf. Ship Drag Reduction (SMOOTH-SHIPS), pp. 93–102, 20–21 May 2010, Istanbul, Turkey.
Kumagai, I., Murai, Y., Tasaka, Y., Nakamura, N., 2011a. Bubble generation by a cylinder moving beneath a free surface. J. Fluid Sci. Technol. 6 (6), 851–859.
Kumagai, I., Kushida, T., Oyabu, K., Tasaka, T., Murai, Y., 2011b. Flow behavior around a hydrofoil close to a free surface. Visual. Mech. Processes 1 (3), http://dx.doi.org/10.1615/VisMechProc.v1.i3.120 (2011).
Mäkiharju, S., Perlin, M., Ceccio, S.L., 2012. On the energy economics of air lubrication drag reduction. Int J. Naval Archit. Ocean Eng. 4, 412–422.
Mizokami, S., Kawakita, C., Kodan, Y., Takano, S., Higasa, S., Shigenaga, R., 2010. Experimental study of air lubrication method and verification of effects on actual hull by means of sea trial. Mitsubishi Heavy Ind. Tech. Rev 47 (3), 41–47.
Murai, Y., 2014. Frictional drag reduction by bubble injection. Exp. Fluids 55 (1773), 28.
Murai, Y., Takahashi, Y., 2008. Frictional drag reduction ship. In: Patent Number: 4070385 (2008), Japan.
Murai, Y., Kumagai, I., Tasaka, Y., Takeda, Y., Takahashi, Y., 2010. Hydrofoil type of bubble generator for marine drag reduction,. Trans. Jpn. Soc. Mech. Eng. Ser. B 76 (763), 483–485.
Ohashi, H. Matsumoto, Ichikawa, Y., Tsukiyama, Y., 1990. Air–water two-phase flow test for airfoil studies. Exp. Fluids 8, 249–256.
Peregrine, D.H., 1983. Breaking waves on beaches. Ann. Rev. Fluid Mech 15, 149–178.
Schlichting, H., 1979. Boundary Layer Theory. McGraw-Hill Series in Mechanical Engineering, McGraw-Hill, New York p. 817.
Takahashi, Y., Murai Y., 2004. Friction reducing ship and method for reducing frictional resistance. In: United States Patent No. US 6,789,491 B2.
Toffoli, A., Babanin, A., Onorato, M., Waseda, T., 2010. Maximum steepness of oceanic waves: field and laboratory experiments. Geophys. Res. Lett. 37, L05603. http://dx.doi.org/10.1029/2009GL041771.
Watanabe, O., Masuko, A., Shirose, Y., 1998. Measurements of drag reduction by microbubbles using very long ship models (in Japanese). J. Soc. Naval Arch. Jpn. 183, 53–63.